The penetration ring is a novel infection structure formed by the penetration peg for invading plant cell membrane in rice blast fungus

Wenqin Fang[1,2,3], Xiaoyu Zai[1,2], Jia Chen[1,2], Yakubu Saddeeq Abubakar[1,2,4], Qiuqiu Wu[1,2], Zhenyu Fang[1,2], Xiuwei Huang[1,2], Xiang Gan[1,2], Daniel J. Ebbole[5], Zonghua Wang[1,2,3,*], Wenhui Zheng[1,2,*]

[1] State Key Laboratory of Ecological Pest Control for Fujian and Taiwan Crops, College of Plant Protection, Fujian Agriculture and Forestry University, Fuzhou, Fujian, 350002, China.

[2] Key Laboratory of Biopesticide and Chemical Biology, Ministry of Education, College of Plant Protection, Fujian Agriculture and Forestry University, Fuzhou, Fujian, 350002, China.

[3] Fuzhou Institute of Oceanography, Minjiang University, Fuzhou 350108, China

[4] Department of Biochemistry, Faculty of Life Sciences, Ahmadu Bello University, Zaria, 810281, Nigeria

[5] Department of Plant Pathology & Microbiology, Texas A&M University, College Station, TX, 77843, USA

* Corresponding author:

Wenhui Zheng (wenhuiz@fafu.edu.cn)

Zonghua Wang (wangzh@fafu.edu.cn)

Author Contributions: D.J.E., Z.W., and W.Z. designed research; W.F., X.Z., J.C., Q.W., Z.F., X.H., X.G., and W.Z. performed research; W.F., Z.W., and W.Z. analyzed data; and W.F., Y.S.A., Z.W., and W.Z. wrote the paper.

Competing Interest Statement: The authors declare no competing interest.

Keywords: penetration ring, secreted protein, *Magnaporthe oryzae*, peg, appressorium

Abstract

Many fungal pathogens develop specialized infection structures such as appressoria to penetrate plant cells. However, it is not clear whether special structures are formed after cell wall penetration before invading host cytoplasm membrane in hemibiotrophic pathogens. Here, we showed that a penetration ring consisting of Ppe1 secreted proteins is formed after appressorium-mediated cell wall penetration and remained at the base of penetration site after invading plant cytoplasm membrane in the rice blast fungus *Magnaporthe oryzae*. The same persistent Ppe1 ring is formed after the penetration of neighboring cells by transpressoria. *PPE1* is specifically expressed during plant infection and the Δ*ppe1* mutant is defective in penetration and invasive growth. Blockage of penetration peg formation impedes the development of the Ppe1 ring. Close examinations showed that the penetration ring is formed at the collar of penetration pegs between plant cell wall and cytoplasm membrane and it is persistent as a fixed ring even after invasive hyphae invaded neighboring cells. Furthermore, Ppe1 is a member of an expanded family of secreted proteins that are unique to fungal pathogens using extreme appressorium turgor for plant penetration. Other members of the Ppe1 family also localize to the penetration ring for anchoring on cytoplasm membrane during plant infection. Taken together, a penetration ring consisting of a family of secreted proteins is formed between plant cell wall and cytoplasm membrane, which may function as a novel physical structure at the interface between the tip of penetration pegs and plant cytoplasm membrane before the differentiation of invasive hyphae.

Significance Statement

Like many other plant pathogens, the rice blast fungus forms melanized appressoria (specialized infection structures) to penetrate plant cells. In this study, we showed that a penetration ring is formed by penetration pegs after appressorium- or transpressorium-mediated penetration of plant cell wall. This ring of secreted proteins is persistent at the point of penetration pegs invading plant cytoplasm membrane to form invasive hyphae. Therefore, after the penetration of plant cell wall, the rice blast fungus forms a penetration ring that consists of a family of secreted proteins unique to pathogens using extreme appressorium turgor for penetration and may function as a physical

53 structure for anchoring onto plant cytoplasm membrane and developing invasive hyphae in
54 penetrated cells.
55
56 **Introduction**
57 *Magnaporthe oryzae*, a filamentous ascomycete, is the causal agent of the devastating rice blast
58 disease, which poses a significant threat to global rice production (1, 2). In addition to rice, *M.*
59 *oryzae* is capable of infecting a wide range of grass species, including major cereal crops such as
60 wheat, barley, oat, and millet, thus compromising global food security (3, 4). As one of the most
61 important plant diseases, it is mainly controlled by planting resistant cultivars. Nevertheless,
62 outbreaks of rice blast still occur throughout rice growing regions worldwide because of
63 breakdown of resistance by new races of the pathogen. In addition, wheat blast caused by *M.*
64 *oryzae* pathovar *Triticum* has recently spread from South America to Asia, threatening wheat
65 production (5, 6).
66
67 Like many other foliar fungal pathogens, penetration of the cuticle and cell wall of host plants is
68 the most critical infection step (7, 8). The infection cycle of *M. oryzae* starts with attachment of
69 dispersing conidia to plant surface by releasing sport tip mucilage. Germ tubes emerging from
70 attached conidia can sense surface hydrophobicity and hardness and develop highly specialized
71 infection structures known as appressoria at the tip (1, 9). Mature dome-shaped appressoria are
72 anchored on rice surface with appressorium mucilage (10) and heavily melanized by depositing a
73 melanin layer between the cell wall and membrane as an impermeable barrier for turgor generation
74 (11). Subsequently, the appressorium uses the extremely high turgor pressure to physically
75 penetrate the cuticle and cell wall with a narrow penetration peg (7, 12, 13). As an hemibiotrophic
76 pathogen, after the penetration of plant cell wall, the penetration peg does not penetrate plant
77 cytoplasm membrane but differentiates into primary invasive hyphae and invasive hyphae that are
78 enveloped by plant-derived extra-invasive hyphal membrane (EIHM) in penetrated cells (7, 14).
79 To date, it is not clear whether there is any special structure at the contact point between the
80 penetration peg and plant cytoplasm membrane before the differentiation of primary invasive
81 hyphae. However, a biotrophic interfacial complex (BIC), a plant membrane-rich structure, is
82 formed at the tip of the primary invasive hyphae for effector delivery (15, 16). Following

83 proliferation within the first colonized cell, the tips of invasive hyphae differentiate into
84 transpressoria, which subsequently form narrow infection pegs to traverse the plasmodesmata
85 (PD)-rich cell junctions, allowing entry into adjacent host cells (17, 18). The fungus continues this
86 colonization strategy until disease symptoms manifest on infected rice plants.
87
88 To suppress plant defense responses and facilitate invasive growth, *M. oryzae* deploys effectors
89 with various functions that can be delivered into host tissues or cells with two secretion systems
90 during infection (19). Apoplastic effectors, such as Bas4 and Slp1, accumulate in the extracellular
91 space between the fungal invasive hyphal cell wall and EIHM, outlining the entire invasive hyphae,
92 are secreted through the conventional endoplasmic reticulum (ER)-Golgi-dependent pathway
93 which is sensitive to brefeldin A (BFA) (19). Conversely, cytoplasmic effectors, including Pwl2,
94 AvrPiz-t, and Bas1, accumulate in the BIC before being delivered into plant cells using a Golgi-
95 independent pathway involving the exocyst complex and t-SNAREs, which is insensitive to BFA
96 (19). To date, all the known proteinaceous effectors in *M. oryzae* belong to these two categories
97 and localize to the extracellular space outlining invasive hyphae or the BICs and intracellular
98 targets inside plant cells.
99
100 In a previous study, we identified a family of small secreted proteins that may function as effectors
101 in *M. oryzae* (20). In this study, we found that one of them named as *PPE1* (for peg periphery-
102 localized effector 1, MGG_16603) is specifically expressed during plant infection and is a crucial
103 virulence factor. Surprisingly, Ppe1 preferentially localizes to the penetration site in a ring
104 conformation that is described as the penetration ring below. The penetration ring consisting of
105 Ppe1 proteins is formed after appressorium- and transpressorium- mediated plant cell wall
106 penetration and remained at the point where penetration pegs transitioning into primary invasive
107 hyphae. Ppe1 homologs are only present in fungal pathogens using extreme appressorium turgor
108 for plant penetration. Other members of the Ppe1 family also localize to the penetration ring that
109 is at the base of primary invasive hyphae outside plant cytoplasm membrane. Taken together, a
110 penetration ring consisting of secreted Ppe1 family proteins is formed between plant cell wall and
111 cytoplasm membrane, which may function as a novel physical structure at the interface between

112 the tip of penetration pegs and plant cytoplasm membrane before the differentiation of invasive
113 hyphae.

114 **Results**

115 **Ppe1 is important for full virulence of *M. oryzae***

116 We previously identified 21 host-adapted effector genes in *M. oryzae* that may play critical roles
117 during rice infection based on *in silico* analyses (20). To explore the functions of these effectors,
118 we selected *PPE1* (MGG_16603) for further functional characterization because its high
119 transcription level during early infection stages as reported (20, 21). We first assayed the
120 expression profile of *PPE1* during infection by qRT-PCR. The result showed that its expression
121 increased during the early stages of plant infection (24-36 hpi) and peaked at 36 hpi (Fig. 1A).
122 Moreover, fluorescence signals of mCherry driven by the *PPE1* promoter indicated that its
123 expression was only observed in matured appressoria and during infection (Fig. 1B). These results
124 were consistent with the transcriptome data, suggesting that Ppe1 is functional during
125 appressorium penetration and plant infection. Ppe1 encodes a 116-aa protein with typical
126 characteristics of fungal effectors, including an N-terminal signal peptide and eight cysteine
127 residues (Fig. S1A). The signal peptide of Ppe1 is functional in directing the secretion of yeast
128 Suc2 invertase in a yeast signal trap system (Fig. S1B), suggesting that Ppe1 is a secreted protein.
129

130 To determine the biological functions of Ppe1 in *M. oryzae,* we generated a *PPE1* gene deletion
131 mutant in the wild-type strain 70-15 (Fig. S1C). Deletion of *PPE1* had no obvious effect on the
132 fungal growth, conidiation, and appressorium formation (Fig. S1D-G). However, in spray infection
133 assays with rice leaves, the Δ*ppe1* mutant was significantly reduced in the number of disease
134 lesions compared to the wild type (Fig. 1C). In wound infection assays, the Δ*ppe1* mutant also was
135 significantly reduced in virulence and formed smaller lesions than the wild type (Fig. 1D). To
136 confirm the role of *PPE1* in virulence, we generated a complemented strain Δ*ppe1*-com that had a
137 copy of the *PPE1* gene ectopically integrated into its genome. In spray or wound infection assays,
138 Δ*ppe1*-com was similar with the wild type in virulence (Fig. 1C-D), indicating a complete recovery
139 in phenotypes. We then conducted rice leaf sheath penetration assays to observe the infection
140 processes. At 32 hpi, over 91% of the appressoria formed by the wild type and the complemented
141 strain had penetrated and developed invasive hyphae in rice cells. Invasive hyphae in most of the

142 penetrated cells (approximately 60%) had more than two branches, and approximately 10% of
143 them had spread into the neighboring cells (Fig. 1E). In contrast, approximately 25% of the
144 appressoria formed by the Δ*ppe1* mutant had no penetration peg. Although 53.5% of these mutant
145 appressoria successfully penetrated into host cells, only 23% of Δ*ppe1* invasive hyphae had more
146 than two branches and less than 4% had spread into adjacent cells (Fig. 1E). These results indicate
147 that the Δ*ppe1* mutant has defects in appressorium penetration, invasive hyphal growth and
148 subsequent spread of invasive hyphae into neighboring plant cells.
149
150 **Ppe1 forms a ring at the base of appressoria during host penetration**
151 To determine the localization of Ppe1 during infection, we expressed a full-length Ppe1-mCherry
152 fusion protein under the control of *PPE1* promoter in both the wild type (70-15) and the Δ*ppe1*
153 mutant. Rice leaf sheaths were then infected with these strains and the localization of Ppe1 was
154 analyzed by confocal microscopy. In these transformants, Ppe1-mCherry signals were observed as
155 a ring underneath the appressoria (likely at the site of the emergence of penetration pegs) at 22 hpi
156 (Fig. 2A, Video S1). The Ppe1-mCherry ring persisted after appressorial penetration and the ring-
157 shaped fluorescence signal of the Ppe1-mCherry was still observed even after the formation of
158 primary and secondary invasive hyphae (Fig. 2B). We further measured the size of this ring and
159 found that the average diameter of the inner cycle of the Ppe1-mCherry ring was 1.53 μm. The
160 width of the Ppe1-mCherry ring varied from 1.79 to 4.78 μm, which is smaller than the width of
161 appressoria (Fig. 2C) and known septin ring (5.9 μm) at the appressorium pore (13). Furthermore,
162 the Ppe1-mCherry fusion protein could be detected by western blot analysis with proteins isolated
163 from infected rice leave (Fig. S2). Because the Ppe1 ring always appears at the point of emergence
164 of the penetration peg, we named this ring structure as penetration ring.
165
166 To confirm the localization of Ppe1, we also generated Ppe1-GFP transformants. Like Ppe1-
167 mCherry, Ppe1-GFP also formed a ring at the penetration site underneath the appressorium (Fig.
168 2D). These results indicate that, irrespective of being fused with mCherry or GFP, Ppe1 localizes
169 to the penetration ring. To avoid possible overexpression or unexpected effects due to ectopic
170 integration of the fusion constructs, we generated a transformant from 70-15 strain in which
171 mCherry was inserted right before the TAA stop codon of the endogenous *PPE1* gene. In the

172 resulting transformant expressing the in situ *PPE1*-mCherry fusion construct, the penetration ring
173 was also observed (Fig. 2E). These results further verify the localization of Ppe1 to the penetration
174 ring during appressorial penetration.
175
176 **Penetration ring is also formed during the penetration of neighboring cells by transpressoria**
177 In *M. oryzae*, appressoria-like structures called transpressoria are formed by invasive hyphae on
178 the wall boundary of the invaded cell in order to penetrate into neighboring cells (17, 18).
179 Therefore, we observed localization of Ppe1 during transpressorium-mediated penetration of plant
180 cells. In the *PPE1*-mCherry transformant, like during appressorial penetration, the penetration ring
181 was observed during transpressoria-mediated penetration of neighboring cells (Fig. 3A). Similarly,
182 we observed the penetration ring in the neighboring cells penetrated by invasive hyphae of the
183 *PPE1*-GFP transformant (Fig. 3B). The Ppe1-mCherry or Ppe1-GFP ring (Fig. 3A and B – zoomed
184 view) appeared to be at the transpressorial penetration point. These results indicate that the
185 penetration ring is also formed during invasive hyphal cell-to-cell penetration. Furthermore,
186 similar localization of Ppe1 to the penetration ring was observed in barley epidermal cells (Fig.
187 3C). Taken together, we conclude that Ppe1 localizes to the penetration ring during appressorium-
188 mediated and transpressorium-mediated plant cell penetrations in *M. oryzae.*
189
190 **Penetration ring is formed on the periphery of the penetration peg**
191 In *M. oryzae*, appressorium-mediated penetration is a septin-dependent process in which septins
192 aggregate and generate a hetero-oligomeric 5.9 μm ring structure at the appressorial pore to re-
193 organize the F-actin cytoskeleton network to promote the emergence of penetration pegs (13).
194 Following the penetration peg formation, septin ring undergoes further constriction into a smaller
195 ring (22). To clarify the precise site of the penetration ring, we expressed Ppe1-mCherry (under
196 the control of the *PPE1* promoter) in a strain expressing Sep3-GFP (Guy11 background) and then
197 observed their spatiotemporal dynamics during rice leaf sheath infection. At 11 hpi, Sep3-GFP big
198 ring was formed at the appressorium pore but the Ppe1-mCherry ring was not observed (Fig. S3A,
199 Video S2). The Ppe1-mCherry ring signal was observed at 16 hpi, after the constriction of Sep3-
200 GFP ring and the former was completely surrounding the latter (Fig. S3B). Subsequently (at 19
201 hpi), the Ppe1-mCherry ring (still surrounding the Sep3-GFP ring) became constricted (Fig. 4A,

202 Fig. S3C, Video S3). However, on impenetrable hydrophobic coverslips, the Sep3-GFP ring was
203 formed normally at the appressorium pore, but the Ppe1-mCherry ring and constriction of Sep3-
204 GFP were not observed (Fig. S4). These results suggest that Ppe1-mCherry ring is formed after
205 the formation of penetration pegs, outside the constricted Sep3-GFP ring.
206
207 Penetration pegs are rich in microfilaments, filasomes and microtubules (23), therefore, it can be
208 labeled by Lifeact-GFP. Hence, we co-expressed Ppe1-mCherry with Lifeact-GFP in 70-15 and
209 observed their positioning in penetration assays with rice leaf sheaths. The Ppe1-mCherry ring was
210 also observed to surround the Lifeact-GFP signal (Fig. 4B, Video S4), indicating that the
211 penetration ring is localized at the periphery of penetration pegs during the initial infection stage.
212 To confirm this observation, we co-expressed the Ppe1-mCherry with cytosolic GFP in 70-15.
213 Using a three-dimensional (3D) volume rendering image constructed by confocal optical z-series
214 images, we found that the Ppe1-mCherry ring was situated around the narrow site between the
215 appressorium and invasive hyphae labeled with GFP (Fig. 4C).
216
217 A previous study showed that callose deposition is dynamic during *M. oryzae* infection and has
218 three different forms: callose-rich papillae underneath appressorium penetration sites, callose
219 collars formed at cell wall crossing sites around the invasive hyphae and callose deposition at
220 plasmodesmata pit fields (24). To investigate whether the penetration ring locates outside the peg,
221 we stained callose deposits with aniline blue to examine the possible positioning of the callose ring
222 underneath the appressorial penetration site and Ppe1-mCherry. We discovered that the Ppe1-
223 mCherry ring was surrounded by the callose ring, exhibiting partial colocalization and close
224 attachment (Fig. 4D, Video S5). Taken together, we conclude that the penetration ring locates at
225 the periphery of penetration peg during the initial appressorium-mediated host penetration.
226
227 **Formation of the penetration ring at the base of penetration pegs after transpressorium**
228 **penetration**
229 To determine the precise localization of the penetration ring during the transpressoria-mediated
230 penetration, we expressed Ppe1-mCherry (under the control of the *PPE1* promoter) in a Sep5-GFP
231 strain and then observed their spatiotemporal dynamics during rice leaf sheath infection. The

232 results showed that Sep5-GFP first displayed a ring structure at the swollen part of the invasive
233 hyphal tip (Fig. S5A), similar to the septin big ring at the appressorium pore. It then exhibited a
234 collar structure at the constricted infection peg site (Fig. S5B-C), which is consistent with a
235 previous report by Sakulkoo (25). Meanwhile, the Ppe1-mCherry ring or collar-like ring was
236 formed outside the Sep5-GFP collar (Fig. S5B-C), indicating that the penetration ring formed
237 during transpressoria-mediated cell-to-cell penetration is positioned outside the penetration peg.
238 Taken together, we conclude that the penetration ring of *M. oryzae* is localized at the periphery of
239 penetration pegs both during appressoria- and transpressoria-mediated host penetrations.
240

241 **Penetration ring formation requires the initiation of penetration peg formation**

242 To further characterize the relationship between the penetration ring and penetration peg, we
243 observed the expression and localization of Ppe1-mCherry in Δ*mst12,* Δ*nox2* and Δ*nox1* mutant
244 strains that are defective in plant penetration (26, 27). In the Δ*mst12* mutant that is defective in
245 both penetration initiation and peg formation, the Ppe1-mCherry fluorescence signal could not be
246 detected. In the Δ*nox2* mutant that is unable to initiate penetration peg formation, the Ppe1-
247 mCherry ring could not be formed but displayed a disorganized mass underneath the appressorium.
248 Interestingly, in the Δ*nox1* mutant that forms normal penetration pegs but is defective in invasive
249 hyphal elongation, the Ppe1-mCherry ring was formed during rice leaf sheath infection (Fig. 5A),
250 indicating that penetration peg formation is a prerequisite for the emergence of the penetration ring.
251 To confirm this observation, the localization of Ppe1-mCherry fusion proteins was observed after
252 inducing appressorium formation on hydrophobic coverslips and cellophane membranes.
253 Although melanized appressoria were formed, we failed to observed the Ppe1-mCherry ring on
254 the impenetrable coverslips (Fig. 5B). However, the penetration ring is formed after the penetration
255 of cellophane membranes (Fig. 5C). These results indicate that initiation of penetration peg
256 formation is necessary for the formation of the penetration ring.
257

258 **Other Ppe proteins also localize to the penetration ring**

259 To determine whether other secreted proteins homologous to Ppe1 also localize to the penetration
260 ring, we used the amino acid sequence of Ppe1 to carry out BLASTp search at the NCBI database
261 to uncover the homolog proteins of Ppe1 and further analyzed their phylogenetic relationships.

262 The Ppe1 homologs only exist in *Magnaporthe* and *Colletotrichum* species, such as the most
263 common cereal phytopathogens *M. oryzae* and *C. graminicola* (Fig. 6A). Remarkably, these fungi
264 are known to form melanized appressoria and deploy extremely high turgor pressure for plant
265 penetration (8). To understand whether other members of the Ppe1 family (Ppe2, Ppe3, Ppe3, Ppe4,
266 Ppe5, and Ppe6) from *M. oryzae* have similar localization as Ppe1, we tagged each of them with
267 mCherry and expressed them individually in the 70-15 background under the control of their native
268 promoters. Examination of their localizations during infection revealed that Ppe2-mCherry, Ppe3-
269 mCherry and Ppe5-mCherry also exhibit a ring structure during appressorium-mediated host
270 penetration, while the fluorescence signals of Ppe4-mCherry and Ppe6-mCherry were hardly
271 observed, possibly due to their low expression (Fig. 6B). Moreover, when MoT-Ppe1 from *M.*
272 *oryzae* pathovar *Triticum* was expressed in *M. oryzae* under the control of its native promoter, the
273 characteristic penetration ring was also observed (Fig. 6B). All these results suggest that the
274 secreted Ppe proteins accumulate at the penetration ring.
275
276 As controls, we also examined the localizations of Bas4, Slp1, Pwl2, and AvrPiz-t. Under the same
277 experimental conditions, Bas4-GFP and Slp1-GFP were observed to uniformly accumulate within
278 the extra-invasive hyphal membrane (EIHM), outlining the entire invasive hyphae, while Pwl2-
279 mCherry and AvrPiz-t-GFP accumulated in the biotrophic interfacial complex (BIC) (Fig. 6C),
280 which is consistent with previous reports (16, 28, 29). EIHM and BIC are specifically associated
281 with invasive hyphae during biotrophic growth. In contrast, Ppe1 localized to the penetration ring
282 at the periphery of penetration pegs (Fig. 6C). Therefore, unlike subcellular localizations of other
283 effectors to the extracellular space outlining invasive hyphae, BICs, or intracellular targets in plant
284 cells, Ppe1 and its homologs localize to the penetration ring that may function as a novel physical
285 structure at the interface between the tip of penetration pegs and plant cytoplasm membrane before
286 the differentiation of invasive hyphae.
287
288 **Discussion**
289 As the model plant pathogenic fungus, appressorium formation and appressorium-mediated
290 penetration have been well-characterized in *M. oryzae* (18). The fungus uses extremely high turgor
291 pressure generated in appressoria cemented to the surface with appressorium mucilage to penetrate

292 underlying plant cells (12). As an hemibiotrophic pathogen, after piercing plant cell wall, the
293 penetration peg does not penetrate the cytoplasm membrane but differentiates into invasive hyphae
294 enveloped in a layer of EIHM (16). In this study, we showed that a penetration ring of Ppe1
295 proteins is formed by the penetration peg on the surface of the plant cytoplasm membrane before
296 invading and differentiating into primary invasive hyphae (Fig. 2 and Fig. 7). Other Ppe proteins
297 including Ppe2, Ppe3, and Ppe5 proteins also localize to the penetration ring (Fig. 6B). Because
298 the penetration ring is persistent at the point penetration pegs transitioning into invasive hyphae
299 outside the cytoplasm membrane even after the penetrated cells are filled with invasive hyphae, it
300 may function as a novel physical structure for anchoring penetration pegs on the surface of plant
301 cytoplasm membrane after cell wall penetration (Fig. 7). It is also possible that this penetration
302 ring functions as a collar or landmark that is associated with the differentiation of penetration pegs
303 (on the surface of cytoplasm membrane) into primary invasive hyphae enveloped in the EIHM
304 cytoplasm membrane (Fig. 7). Although this transition is not well characterized, it likely involves
305 changes in cell polarity and cytoskeleton as well as cell wall modifications. Ppe1 and its homologs
306 may be able to assemble into a protein complex in the penetration ring, which likely involves other
307 proteins or components as facilitating factors. In *U. maydis*, the Stp secreted effectors are known
308 to form a protein complex during plant infection (30).
309

310 The penetration ring is also formed after transpressoria-mediated penetration of neighboring plant
311 cells (Fig. 7). Similarly, Ppe1 and its homologs form a ring after the penetration of cell wall but
312 before differentiating into invasive hyphae enveloped with the EIHM. The penetration ring formed
313 by transpressoria-mediated penetration is also persistent at the penetration site on the surface of
314 plant cytoplasm membrane in penetrated cells (Fig. 3 and Fig. S5), suggesting that Ppe proteins
315 are assembled into a complex that is not diffusible. In fact, similar penetration ring is observed
316 after penetration of artificial membrane (Fig. 5C), which has no barrier to restrict the diffusion of
317 secreted proteins, further indicating that the penetration ring of Ppe1 and other Ppe proteins is
318 likely a structural feature or component for signaling the transition of penetration pegs to invasive
319 hyphae. Although appressoria and transpressoria are different, the processes after the penetration
320 of cell wall are the same in appressorium- and transpressorium-mediated plant penetration.

321 Therefore, formation of the penetration ring in both appressorium- and transpressorium-mediated
322 penetration is another evidence for it to be a structural element.

323 *M. oryzae* is known to secrete a repertoire of effectors that can be categorized into cytoplasmic
324 and intracellular effectors (14). Ppe1 and its homologs are putative effectors that are described as
325 HAG (host adaptation genes) effectors in an earlier study (20). Although it remains possible that
326 Ppe1 and its homologs function as effectors during plant infection. However, in comparison with
327 the localizations of known effectors in *M. oryzae*, we found that the localization of Ppe1 to the
328 penetration ring is unique and Ppe1 homologs have the same localization pattern (Fig. 6). Because
329 of the persistent localization of Ppe1 and its homologs to the penetration ring, we think the
330 penetration ring is likely a physical structure as described above. If Ppe1 and its homologs are
331 effector proteins being secreted at this specific location, fluorescent signals of Ppe1 and its
332 homologs will diffuse and disappear or dimmish when effectors being translocated into plant cells.
333 Furthermore, it is unlikely that secreted proteins localized to the penetration ring that has limited
334 contact with the plant cytoplasm membrane will function as effector proteins to interact with plant
335 targets. Nevertheless, although unlikely, it remains possible that the penetration ring discovered in
336 this study is a secretion site for effectors involved in the transition of penetration pegs to invasive
337 hyphae. After the penetration of plant cell wall, the penetration ring may not only function as a
338 physical structure but also serve as an initial effector secretion site for the release of specific
339 effectors to overcome plant immunity in early infection stages.

340 Taken together, in this study we observed the formation of the penetration ring that appears to be
341 a structural element for signaling or triggering the differentiation of penetration pegs after the
342 penetration of plant cell wall into invasive hyphae enveloped by the EIHM in *M. oryzae*. Based on
343 the limited distribution of Ppe1 homologs, it is likely that only fungal pathogens using high
344 appressorium turgor for plant penetration, such as *M. oryzae* and *Colletotrichum* species,
345 developed the penetration ring. Therefore, it will be important to further characterize the functional
346 relationship between the penetration ring and appressorium turgor as well as the transition of
347 penetration pegs driven by turgor pressure into primary invasive hyphae (lower turgor pressure).

348

349 **Materials and Methods**

350 **Strains and growth conditions**

351 The *M. oryzae* strains 70-15 and Guy11 were used as the wild types in this study; all other fungal
352 strains generated from the wild types are listed in Table S1 in the supplemental materials. All the
353 fungal strains were grown on complete medium CM (CM: 10 g D-glucose, 2 g peptone, 1 g yeast
354 extract, 1 g casamino acids, 50 mL 20 × nitrate salts (120 g/L $NaNO_3$, 10.4 g/L KCl, 30 g/L
355 KH_2PO_4, and 10.4 g/L $MgSO_4$), 1 mL trace elements (0.1 g/L biotin, 0.1 g/L pyridoxine, 0.1 g/L
356 thiamine, 0.1 g/L riboflavin, 0.1 g/L p-aminobenzonic acid and 0.1 g/L nicotinic acid), adjusted to
357 pH 6.5 with NaOH, 15 g agar and distilled water added to 1 L) (31). Agar cultures were incubated
358 at 26 °C with a 12-h light/12-h dark photoperiod for mycelial growth and conidiation. Liquid CM
359 medium was used to harvest mycelia for extraction of genomic DNA and protoplast preparation.
360 The bacterial strains *Escherichia coli* DH5α and *Agrobacterium tumefaciens* AGL1 were grown
361 in Luria-Bertani (LB) medium at 37 °C and 28 °C, respectively.

362

363 **Plant and growth conditions**

364 Rice cultivar CO-39 (*Oryza sativa* cv. CO-39) was grown in a greenhouse at 26 °C and 70%
365 relative humidity with a 14-h light/10-h dark photoperiod. Barley (*Hordeum vulgare* cv. Golden
366 Promise) was grown at 23 °C with a 12-h light /12-h dark photoperiod.

367

368 **Bioinformatic and phylogenetic analyses of Ppe1 homolog proteins**

369 The Ppe1 was previously sequenced and the amino acid sequence established from our lab (32).
370 Ppe1 signal peptide was predicted using SignalP 5.0 software. BLASTp was used to find Ppe1
371 homolog proteins at the NCBI database (https://www.ncbi.nlm.nih.gov/) and the representative
372 homolog protein sequences were downloaded from the database. Phylogenetic tree was generated
373 using MEGA7.0 software by neighbor-joining method.

374

375 **Construction of recombinant DNA and *M. oryzae* transformation**

376 The plasmids used in the study were generated by infusion cloning method based on homologous
377 recombination using ClonExpress II one-step cloning kit or ClonExpress MultiS kit (Cat. No.
378 C112-01 or C113-01, Vazyme, Nanjing, China). The primers used (Table S2 in the supplemental
379 material) were specially designed to contain 18-22-bp overlap with adjoining sequences to allow

380 the fragments assemble by homologous recombination. To observe the expression pattern and
381 localization of *PPE1*, the *PPE1* promoter (1485 bp) fragment amplified from the genomic DNA
382 of the wild type (70-15) was seamlessly cloned into the *Kpn*I/*Hin*dIII-digested pKNT-
383 mCherry/GFP fusion vectors (33) using the ClonExpress II one-step cloning kit (Cat. No. C112-
384 01, Vazyme, Nanjing, China). For Ppe1-mCherry/GFP plasmid, the entire Ppe1 coding sequence
385 with its native promoter but without stop codon was amplified and cloned into the *Kpn*I/*Hin*dIII-
386 digested vector pKNT-mCherry/GFP. The pKNT-AvrPizt-GFP and other plasmids used were was
387 constructed using the same method. The constructed plasmids were transformed into the fungal
388 protoplasts via PEG-mediated transformation (34) and further verified by PCR screening and
389 confocal microscopic examination of fluorescence signals. For situ fusion of Ppe1 with mCherry,
390 the mCherry was inserted just before the Ppe1 stop codon and the construct was transformed by
391 *Agrobacterium tumefaciens*-mediated (ATMT) transformation for homologous recombination
392 (34).
393
394 **Assays for the secretory function of the SP of Ppe1**
395 To confirm the secretory function of the predicted signal peptide (SP), yeast signal trap system
396 was performed as described previously (35). The predicted SP nucleotide sequences of Ppe1 (60
397 bp) and Pwl2 (63 bp) were respectively cloned into pSUC2 vector that carries a truncated invertase
398 gene *SUC2.* The generated pSUC2-SP constructs and the empty pSUC2 vector were transformed
399 into the yeast *suc2* mutant YTK12, respectively, and then their growth conditions analyzed on
400 CMD-W (minus Trp) plates (0.67% yeast nitrogen base without amino acids, 0.075% tryptophan
401 dropout supplement, 2% sucrose, 0.1% glucose, and 2% agar) and YPRAA medium plate (1%
402 yeast extract, 2% peptone, 2% raffinose, and 2 μg/mL antimicyn A) containing raffinose and
403 lacking glucose. Transformants of YTK12 carrying the empty pSUC vector or pSUC2-Pwl2SP
404 were used as negative and positive controls, respectively. Reduction of 2,3,5-triphenyltetrazolium
405 chloride (TTC) to insoluble red-colored 1,3,5-triphenylformazan (TPF) was used as an indicator
406 of the invertase enzymatic activity (36). Each of the above YTK12 transformants strain was
407 inoculated in 5 mL of CMD-W liquid medium and incubated for 24 h at 30 ℃. The cells were then
408 collected, washed and resuspended in 0.1% TTC in new centrifuge tubes and further incubated at

409 35 °C for 35 min. The color change was observed after 10 min of incubation at room temperature
410 to detect the signal peptide secretion function.
411
412 **Targeted gene deletion and complementation**
413 Deletions of *NOX1*, *NOX2* and *MST12* genes were performed using Split-marker recombination
414 method (37). The open reading frames (ORFs) of the various genes were replaced with a
415 hygromycin phosphotransferase (*HPH*) resistance cassette, respectively. Briefly, about 1-kb
416 upstream and downstream sequences of the targeted genes were amplified from the genomic DNA
417 of the wild type (70-15) using specially designed primer pairs AF+AR and BF+BR, respectively.
418 At the same time, the upstream and downstream sequences of the *HPH* with overlapping segments
419 were amplified from pCB1003 plasmid using the primer pairs HYG/F + HY/R and YG/F + HYG/R,
420 respectively. The corresponding upstream and downstream fragments were respectively ligated by
421 splicing for overlap extension (SOE) PCR using the primer pairs AF+HY/R and YG/F+BR. The
422 PCR products were purified and transformed into the Ppe1-mCherry strain protoplasts via a PEG-
423 mediated transformation (34). Putative transformants were selected in the presence of hygromycin
424 B and then confirmed by PCR using the primers OF+OR and UA+H853. PCR confirmations were
425 repeated three times for consistency. All the primer sequences used are listed in Table S2 of the
426 supplemental material.
427
428 For *PPE1* gene deletion, *HPH* sequence was inserted between the upstream and downstream
429 sequences of the *PPE1* gene, replacing the ORF of the *PPE1* gene, in an ATMT1 plasmid using a
430 ClonExpress MultiS One Step Cloning Kit (Cat. no. C113-01, Vazyme, Nanjing, China). The
431 constructed plasmid was introduced into *Agrobacterium tumefaciens* AGL1 using freeze-thaw
432 method (38). *Agrobacterium tumefaciens*-mediated transformation (ATMT) of the construct into
433 the wild-type spores was then carried out. The transformants were selected on hygromycin B plates
434 and confirmed by PCR. The mutants were further confirmed by Southern blot assay using DIG-
435 High Prime DNA labeling and detection starter kit I (Cat. no. 11745832910, Roche, Mannheim,
436 Germany). For complementation, the constructed plasmid pKNT-Ppe1-mCherry was transformed
437 into the Δ*ppe1* mutant protoplast and further verified by PCR screening and confocal microscopic
438 examination for fluorescence signal detection.

439

440 **Live cell imaging**

441 To monitor the expression and subcellular localization of Ppe1 during plant infection, rice leaf
442 sheath inoculation and live cell imaging of fluorescently labeled proteins were performed as
443 described (15) with slight modifications. In brief, 5-7 cm long leaf sheath segments were cut from
444 4-week-old CO-39 rice seedlings, and the whole hollow spaces of the sheaths were filled with
445 conidia suspensions (5×10^4 conidia/mL) using a 200 μL pipette. The inoculated sheaths were
446 placed horizontally (fixed with wet filter paper fragments) on an inverted 96-well PCR plate
447 covered by one layer of wet filter paper and incubated in a sealed box whose inner bottom was
448 lined with two layers of wet filter paper to keep the environment humid at 26 °C. The epidermal
449 parts of the inoculated sheaths were trimmed into thin and transparent samples and immediately
450 imaged using an inverted Nikon A1 laser scanning confocal microscope (Nikon, Tokyo, Japan) at
451 the indicated time points post inoculation. The 60×/1.42 numerical aperture (NA) oil immersion
452 objective lens was used for the imaging. The fluorescence and differential interference contrast
453 (DIC) images were collected by confocal optical z-series acquired at 0.28 μm intervals spanning
454 the entire fluorescence signal depth between the top plane of the appressorium formed and the
455 bottom plane of the rice leaf sheath cross sections. The fluorescence excitation/emission
456 wavelengths were 488 nm/500-550 nm for GFP, 561 nm/570-620 nm for mCherry and 405
457 nm/425-475 nm for callose staining. The images were processed using NIS-Elements AR analysis
458 software (Nikon, Tokyo, Japan). Unless otherwise stated in the figure legend, micrograph
459 fluorescence represents maximum intensity projection of z-series (with a 0.28 μm intervals) after
460 removing extraneous z-planes that do not contain relevant information for a particular fluorescence.
461 Three-dimensional (3D) volume rendering images and videos were generated from z-series in
462 maximum intensity projection.

463

464 To observe the subcellular localizations of Ppe1 in conidia incubated on artificial hydrophobic
465 surfaces and barley leaves, conidia suspensions (5×10^4 conidia/mL) were dropped on the surfaces
466 of hydrophobic coverslips or on the back sides of barley leaves (5-day old plants) and incubated
467 under humid and dark conditions at a 26 °C. For observation, the hydrophobic coverslips
468 containing the appressoria were inverted, placed on 24mm×50 mm microscope glass slides and

469 then observed under a scanning confocal microscope. Epidermal parts were removed from the
470 infected barley leaves for observation. For penetration assay, cellophane was cut into round sheets
471 of 4 cm in diameter and sterilized by autoclaving at 115 ℃ for 15 min. The sterile cellophane
472 sheets were placed flat on CM plates and then the conidia suspensions (5×10^4 conidia/mL) were
473 dropped on the surface of the cellophane and incubated at 26 ℃. Small pieces of the cellophane
474 containing mycelia were cut for observation under a confocal microscope at 36-48 hpi.
475
476 **Callose staining**
477 For visualization of deposited callose, aniline blue (Cat. no. 28631-66-5, Sangon, Shanghai, China)
478 staining was adopted (25). Rice leaf sheaths were inoculated with conidia suspensions (3×10^4
479 conidia/mL). The inoculated sheaths were trimmed to thin and transparent samples at the indicated
480 time points and stained with aniline blue (0.1mg/mL) solution prepared in 150 mM KH_2PO_4 (pH
481 9.5) for up to 30 min. The stained samples were imaged by using a laser scanning confocal
482 microscope (Nikon, Japan).
483
484 **Phenotypic analysis**
485 For vegetative growth and conidiation assays, small mycelial blocks from each strain were cut
486 from the edges of 4-day-old cultures and placed at the center of freshly prepared CM plates (90
487 mm) and incubated for ten days at 26 ℃. The colony diameters of the cultures were measured
488 using vernier calipers and then photographs of the cultures were taken. The cultures were then
489 washed with 5 mL sterilized double-distilled water, filtered through three layers of lens paper and
490 the conidia counted using a hemocytometer under a light microscope. For conidia germination and
491 appressoria formation, spore suspensions (1×10^5 conidia/mL) were incubated on hydrophobic
492 coverslips (Cat. no. 12-545-101P, Fisherbrand™ Cover Glasses, USA) under humid and dark
493 conditions at 26 ℃ for 24 h. The conidia were then observed under a light microscope for
494 germination and formation of appressoria.
495
496 To investigate the pathogenicity of each strain, conidia spray, punch and leaf sheath inoculations
497 were performed. Conidia suspensions (5×10^4 conidia/mL containing 0.02% Tween-20) were used
498 to spray the leaf surfaces of 3-week-old CO-39 rice seedlings. The inoculated seedlings were

499 incubated in a growth chamber at 25 °C with 90% humidity. The seedlings were first kept in the
500 dark for 24 h, and then subjected to 12 h light / 12 h dark photoperiod for 7 days, after which
501 photographs were taken and the number of disease lesions on the leaf surfaces counted. Punch
502 inoculation assay was carried out according to a method previously described (29). Briefly, 5-
503 week-old CO-39 rice leaves were slightly wounded using mouse ear punch and 10 μL of conidia
504 suspensions (5×10^5 conidia/mL containing 0.02% Tween-20) from the various strains were
505 respectively dropped at the wounded regions. Then, both sides of each inoculated spot were sealed
506 with scotch tape to sustain the spore suspension. The inoculated plants were kept in a growth
507 chamber under the same conditions described above for 10 days. The disease lesions formed were
508 scanned, and later analyzed using Adobe Photoshop software to measure the lesion areas. For leaf
509 sheaths inoculation, conidia suspensions (1×10^5 conidia/mL) from the various strains were
510 respectively injected into 4-5 weeks old CO-39 rice leaf sheaths. The epidermal parts of the
511 infected leaves were trimmed to thin and transparent samples for observation under a light
512 microscope at 32 hpi. At least 100 infected sites were observed using a Nikon A1 laser confocal
513 microscope (Nikon, Tokyo, Japan).
514
515 **qRT-PCR analysis**
516 To analyze the expression level of *PPE1* during *M. oryzae* infection, rice leaf sheaths were cut
517 from 4- to 5-week-old CO-39 rice seedings and inoculated with conidia suspensions (2×10^5
518 conidia/mL) from the wild type (70-15). The epidermal parts of the inoculated sheaths were cut
519 and collected at 12-, 36- and 48 hours post inoculation (hpi). At least 15 segments of the inoculated
520 rice sheath samples were collected at each time point. Total RNAs were extracted from the leaf
521 sheaths or rice seeding leaves using an Eastep Super Total RNA Extraction Kit (Cat. no. LS1040,
522 Promega, Shanghai, China). Reverse transcription was used to generate cDNA using a reverse
523 transcription kit (Cat. no. RR037B, Takara, Dalian, China). Quantitative PCR was finally
524 conducted using a SYBR kit (Cat. no. RR067A, Takara, Dalian, China) using specific primers
525 (Table S2). Fugal *β-TUBULIN* gene used as endogenous reference genes, and the expression levels
526 were calculated using $2^{-\Delta\Delta Ct}$ method as previously reported (39). All qRT-PCR assays were
527 repeated three times for each sample.
528

529 **Statistical analyses**

530 Statistical analyses were performed using GraphPad Prism7 (GraphPad Software, Inc., San Diego,
531 CA). Statistically significant differences were determined by one-way ANOVA with two-sided
532 least significant difference. **** indicated significant difference at $p < 0.0001$， ns indicated no
533 significant difference.

534

535 **Data Availability**

536 The authors declare that all the data supporting the findings of this study are available within the
537 paper and SI Appendix. Raw data and details of experimental procedures are available upon
538 request from the corresponding authors.

539

540 **Acknowledgments**

541 We thank Prof. Nicholas J. Talbot and Prof. Barbara Valent for providing us with *Δsec5* mutant
542 and pBV591 plasmid respectively. We also thank Prof. Min Guo for providing us with Sep3/5-
543 GFP strains and Δsep3/4/5 mutants. We also appreciate Profs. Guodong Lu, Jie Zhou, Huawei
544 Zheng, Wei Tang, Ya Li, Xiaofeng Chen, and Huakun Zheng, as well as Drs Yijuan Hang, Meilian
545 Chen and Yonghe Hong for their helpful suggestions. Thanks to Jin Zhang, Chunling Li and
546 Yuping Fan's help. This research was supported by the National Key Research and Development
547 Program of China (2023YFD1400200), the National Natural Science Foundation of China
548 (32122071, 31601596), and the Natural Science Foundation of Fujian Province (2021J06015).

549

550

551 **References**

552 1. Talbot NJ (2003) On the trail of a cereal killer: Exploring the biology of Magnaporthe grisea.
553 *Annual review of microbiology* 57:177-202.
554 2. Dean R*, et al.* (2012) The Top 10 fungal pathogens in molecular plant pathology. *Molecular plant*
555 *pathology* 13(4):414-430.
556 3. Couch BC*, et al.* (2005) Origins of host-specific populations of the blast pathogen Magnaporthe
557 oryzae in crop domestication with subsequent expansion of pandemic clones on rice and weeds
558 of rice. *Genetics* 170(2):613-630.
559 4. Langner T, Białas A, & Kamoun S (2018) The Blast Fungus Decoded: Genomes in Flux. *mBio* 9(2).
560 5. Ceresini PC*, et al.* (2018) Wheat Blast: Past, Present, and Future. *Annual review of*
561 *phytopathology* 56:427-456.

562 6. Malaker PK*, et al.* (2016) First Report of Wheat Blast Caused by Magnaporthe oryzae Pathotype
563 triticum in Bangladesh. 100(11):2330-2330.
564 7. Howard RJ & Valent B (1996) Breaking and entering: host penetration by the fungal rice blast
565 pathogen Magnaporthe grisea. *Annual review of microbiology* 50:491-512.
566 8. Talbot NJ (2019) Appressoria. *Current biology : CB* 29(5):R144-r146.
567 9. Hamer JE, Howard RJ, Chumley FG, & Valent B (1988) A mechanism for surface attachment in
568 spores of a plant pathogenic fungus. *Science (New York, N.Y.)* 239(4837):288-290.
569 10. Rocha RO, Elowsky C, Pham NTT, & Wilson RA (2020) Spermine-mediated tight sealing of the
570 Magnaporthe oryzae appressorial pore-rice leaf surface interface. *Nature microbiology*
571 5(12):1472-1480.
572 11. Chumley FG & Valent BJMP-mI (1990) Genetic analysis of melanin-deficient, nonpathogenic
573 mutants of Magnaporthe grisea. 3:135-143.
574 12. de Jong JC, McCormack BJ, Smirnoff N, & Talbot NJ (1997) Glycerol generates turgor in rice blast.
575 *Nature* 389(6648):244-244.
576 13. Dagdas YF*, et al.* (2012) Septin-mediated plant cell invasion by the rice blast fungus,
577 Magnaporthe oryzae. *Science (New York, N.Y.)* 336(6088):1590-1595.
578 14. Fernandez J & Orth K (2018) Rise of a Cereal Killer: The Biology of Magnaporthe oryzae
579 Biotrophic Growth. *Trends in microbiology* 26(7):582-597.
580 15. Kankanala P, Czymmek K, & Valent B (2007) Roles for rice membrane dynamics and
581 plasmodesmata during biotrophic invasion by the blast fungus. *The Plant cell* 19(2):706-724.
582 16. Khang CH*, et al.* (2010) Translocation of Magnaporthe oryzae effectors into rice cells and their
583 subsequent cell-to-cell movement. *The Plant cell* 22(4):1388-1403.
584 17. Cruz-Mireles N, Eseola AB, Osés-Ruiz M, Ryder LS, & Talbot NJ (2021) From appressorium to
585 transpressorium-Defining the morphogenetic basis of host cell invasion by the rice blast fungus.
586 *PLoS pathogens* 17(7):e1009779.
587 18. Ryder LS*, et al.* (2022) The appressorium at a glance. *Journal of cell science* 135(14).
588 19. Giraldo MC*, et al.* (2013) Two distinct secretion systems facilitate tissue invasion by the rice blast
589 fungus Magnaporthe oryzae. *Nature communications* 4:1996.
590 20. Ebbole DJ*, et al.* (2021) Evolution and Regulation of a Large Effector Family of Pyricularia oryzae.
591 *Molecular plant-microbe interactions : MPMI* 34(3):255-269.
592 21. Yan X*, et al.* (2023) The transcriptional landscape of plant infection by the rice blast fungus
593 Magnaporthe oryzae reveals distinct families of temporally co-regulated and structurally
594 conserved effectors. *The Plant cell* 35(5):1360-1385.
595 22. Eisermann I & Talbot NJ (2024) Septin-dependent invasive growth by the rice blast fungus
596 Magnaporthe oryzae. *Journal of Plant Diseases and Protection*.
597 23. Bourett TM & Howard RJ (1992) Actin in penetration pegs of the fungal rice blast
598 pathogen,Magnaporthe grisea. *Protoplasma* 168(1-2):20-26.
599 24. Osés-Ruiz M*, et al.* (2021) Appressorium-mediated plant infection by Magnaporthe oryzae is
600 regulated by a Pmk1-dependent hierarchical transcriptional network. *Nature microbiology*
601 6(11):1383-1397.
602 25. Sakulkoo W*, et al.* (2018) A single fungal MAP kinase controls plant cell-to-cell invasion by the
603 rice blast fungus. *Science (New York, N.Y.)* 359(6382):1399-1403.
604 26. Park G, Xue C, Zheng L, Lam S, & Xu JR (2002) MST12 regulates infectious growth but not
605 appressorium formation in the rice blast fungus Magnaporthe grisea. *Molecular plant-microbe*
606 *interactions : MPMI* 15(3):183-192.

607 27. Ryder LS*, et al.* (2013) NADPH oxidases regulate septin-mediated cytoskeletal remodeling during
608 plant infection by the rice blast fungus. *Proceedings of the National Academy of Sciences of the*
609 *United States of America* 110(8):3179-3184.
610 28. Mentlak TA*, et al.* (2012) Effector-mediated suppression of chitin-triggered immunity by
611 magnaporthe oryzae is necessary for rice blast disease. *The Plant cell* 24(1):322-335.
612 29. Park CH*, et al.* (2012) The Magnaporthe oryzae effector AvrPiz-t targets the RING E3 ubiquitin
613 ligase APIP6 to suppress pathogen-associated molecular pattern-triggered immunity in rice. *The*
614 *Plant cell* 24(11):4748-4762.
615 30. Ludwig N*, et al.* (2021) A cell surface-exposed protein complex with an essential virulence
616 function in Ustilago maydis. *Nature microbiology* 6(6):722-730.
617 31. Talbot NJ, Ebbole DJ, & Hamer JE (1993) Identification and characterization of MPG1, a gene
618 involved in pathogenicity from the rice blast fungus Magnaporthe grisea. *The Plant cell*
619 5(11):1575-1590.
620 32. Zhong Z*, et al.* (2018) Population genomic analysis of the rice blast fungus reveals specific events
621 associated with expansion of three main clades. *The ISME journal* 12(8):1867-1878.
622 33. Chen X*, et al.* (2021) Trehalose Phosphate Synthase Complex-Mediated Regulation of Trehalose
623 6-Phosphate Homeostasis Is Critical for Development and Pathogenesis in Magnaporthe oryzae.
624 *mSystems* 6(5):e0046221.
625 34. Khang CH, Park SY, Rho HS, Lee YH, & Kang S (2006) Filamentous Fungi (Magnaporthe grisea and
626 Fusarium oxysporum). *Methods in molecular biology (Clifton, N.J.)* 344:403-420.
627 35. Jiang C*, et al.* (2020) An orphan protein of Fusarium graminearum modulates host immunity by
628 mediating proteasomal degradation of TaSnRK1α. *Nature communications* 11(1):4382.
629 36. Oh SK*, et al.* (2009) In planta expression screens of Phytophthora infestans RXLR effectors reveal
630 diverse phenotypes, including activation of the Solanum bulbocastanum disease resistance
631 protein Rpi-blb2. *The Plant cell* 21(9):2928-2947.
632 37. Kershaw MJ & Talbot NJ (2009) Genome-wide functional analysis reveals that infection-
633 associated fungal autophagy is necessary for rice blast disease. *Proceedings of the National*
634 *Academy of Sciences of the United States of America* 106(37):15967-15972.
635 38. Holsters M*, et al.* (1978) Transfection and transformation of Agrobacterium tumefaciens.
636 *Molecular & general genetics : MGG* 163(2):181-187.
637 39. Livak KJ & Schmittgen TD (2001) Analysis of relative gene expression data using real-time
638 quantitative PCR and the 2(-Delta Delta C(T)) Method. *Methods (San Diego, Calif.)* 25(4):402-
639 408.
640 40. Dean RA*, et al.* (2005) The genome sequence of the rice blast fungus Magnaporthe grisea.
641 *Nature* 434(7036):980-986.

642

643

644

645

646

647 **Figures and Tables**

648

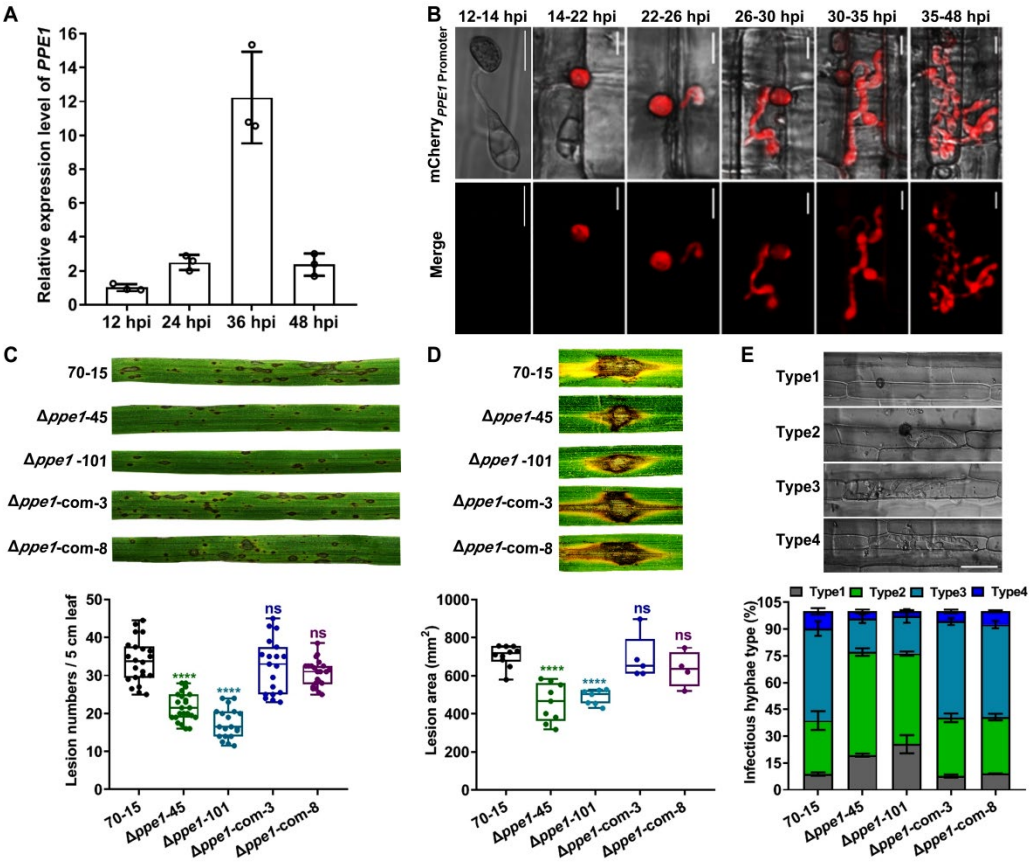

649

650 Fig. 1 Ppe1 is important for full virulence in *M. oryzae*. (A) The relative expression level of Ppe1
651 during infection of rice leaf sheaths assayed by qRT-PCR. (B) Fluorescence signals of the P_{PPE1}-
652 mCherry transformant in penetration assays with rice leaf sheaths. Scale bars = 10 μm. (C) Typical
653 leaves of CO-39 seedlings sprayed with conidia of the wild type (70-15), *PPE1* gene deletion
654 mutants (Δ*ppe1-45*, Δ*ppe1-101*) and complement strains (Δ*ppe1-com-3*, Δ*ppe1-com-8*) examined
655 at 7 days post inoculation (dpi). Boxplot below shows the number of disease lesions per 5 cm of
656 individual inoculated leaf. n = 22, 23, 19, 19, and 22, respectively. (D) Wounded leaves of CO-39
657 drop-inoculated with the marked strains were examined at 10 dpi (upper panel) and measured for

658 the lesion area (lower panel). n = 10, 9, 7, 5, and 4 respectively. (E) Rice leaf sheath penetration
659 assays. Conidia suspensions from each strain were respectively injected into 4-5 weeks old rice
660 leaf sheaths. Infection levels were observed at 32 hpi (hours post inoculation). The infection levels
661 were grouped into four types: Type 1, appressorium formation without penetration; Type 2, having
662 penetration peg or primary invasive hyphae; Type 3, having more than two branched invasive
663 hyphae restricted in the first infected rice cell; Type 4, having invasive hyphae crossing to
664 neighboring host cells. Scale bar = 10 μm. Statistical analyses of the infection types and
665 percentages are also shown. Significant differences were determined by one-way ANOVA.
666 Asterisks indicated significant differences ($p<0.0001$). ns indicated no significant difference
667 ($p>0.05$).

668

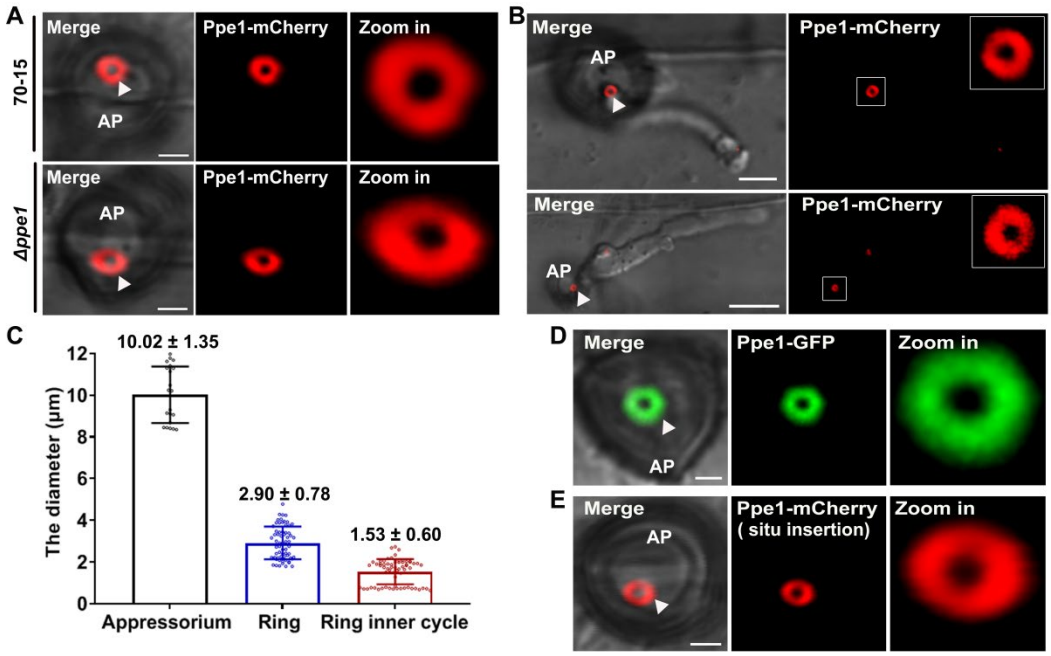

669

670 Fig. 2 Ppe1-mCherry forms a ring during appressorial penetration. (A) A ring of Ppe1-mCherry
671 signals at the penetration site was observed at 22 hpi in leaf sheath penetration assays with the
672 *PPE1*-mCherry transformant. Upper panel indicates the Ppe1-mCherry expressed in wild-type
673 strain (70-15). Lower panel indicates the Ppe1-mCherry expressed in Δ*ppe1* mutant. Scale bars =
674 2 μm. (B) The Ppe1-mCherry penetration ring was persist even after the growth of primary and

675 secondary invasive hyphae. Scale bars = 5 μm. (C) The diameters of appressoria, Ppe1-mCherry
676 penetration ring (ring), and its inner cycle. n= 21, 65 and 65 respectively. (D) The formation of
677 Ppe1-GFP rings at the penetration site formed by the *PPE1*-GFP transformant. Scale bars = 2 μm.
678 (E) The in-situ *PPE1*-mCherry transformant also formed a fluorescent ring at the penetration site
679 in leaf sheath penetration assays. Scale bar = 2 μm. AP, Appressorium. Triangle arrows pointed to
680 penetration rings.

681

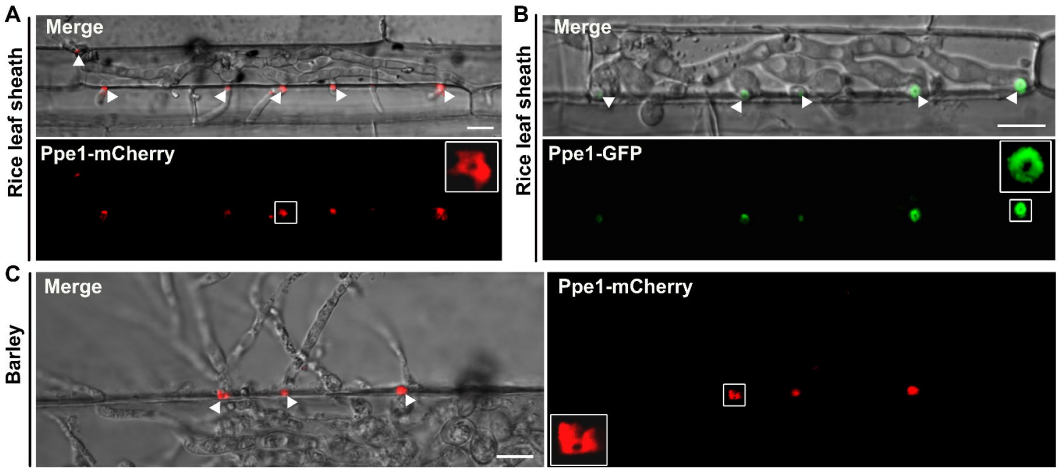

682

683 Fig. 3 Penetration ring formation during invasive hyphal penetration into neighboring cells. (A)
684 Ppe1-mCherry forms rings at about 36 hpi. (B) Ppe1-GFP also forms rings similar to Ppe1-
685 mCherry during penetration to neighboring cells. (C) Ppe1 ring formation is also observed during
686 barley infection. Scale bars = 10 μm. Arrows heads point to penetration rings at the penetration
687 sites of invasive hyphae. White squares indicate zoomed regions.

688

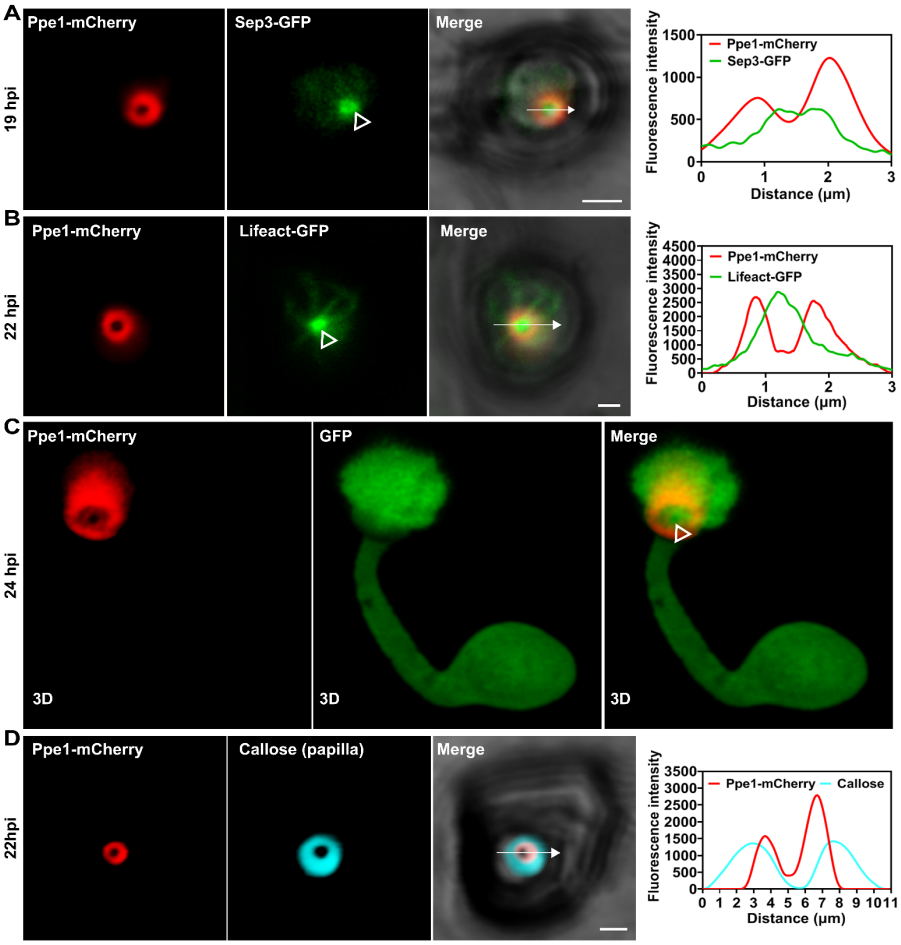

Fig. 4 The penetration ring localizes on the periphery of penetration peg. (A) Ppe1 ring surrounds the Sep3 constricted ring. Scale bar = 2 μm. (B) Ppe1 ring also surrounds the Lifeact ring. Scale bar = 1 μm. (C) Ppe1 ring is formed around the narrow site between an appressorium and invasive hypha. Three-dimensional (3D) volume rendering images were constructed by confocal optical z-series images captured at 0.35 μm intervals, with a total of 22 steps. (D) Ppe1 ring partly colocalized with callose ring at the apoplastic papilla. Scale bar = 1 μm. Hollow triangles indicate the site of penetration peg. Line graphs were generated at the directions pointed by the white arrows.

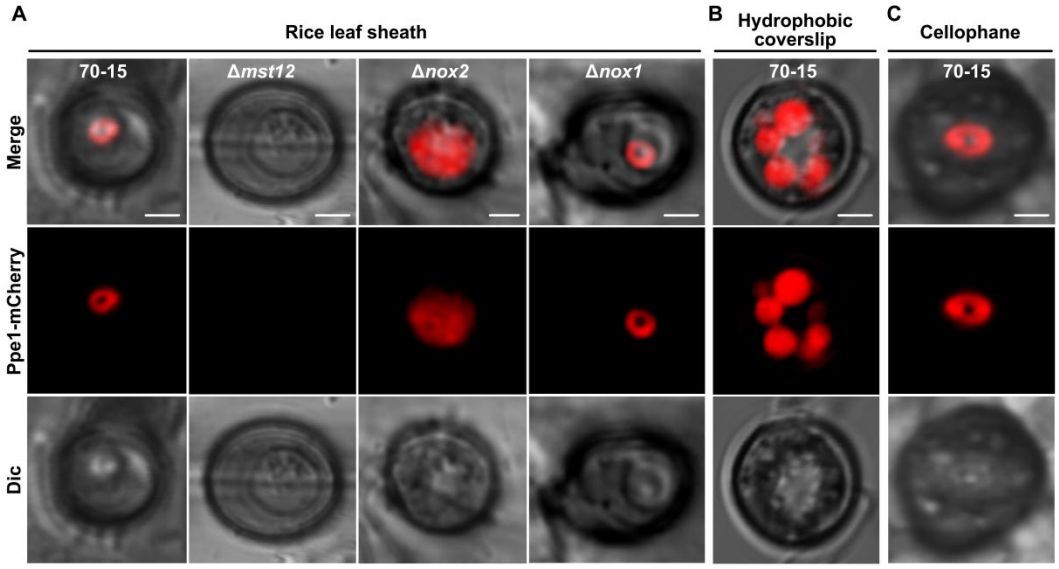

Fig. 5 Penetration ring formation requires the emergence of penetration peg. (A) Ppe1 ring expression and localization in 70-15, Δ*mst12*, Δ*nox2* and *Δnox1* strains at 24 hpi. Conidia suspensions from each strain were inoculated on rice leaf sheaths and observed at 24 hpi. (B) Ppe1 ring could not be formed on impenetrable coverslips. Conidia from Ppe1-mCherry strain were inoculated on hydrophobic coverslips and observed at 24 hpi. (C) Ppe1 ring was observed at 38 hpi on penetrable cellophane membrane. Scale bars = 2 μm.

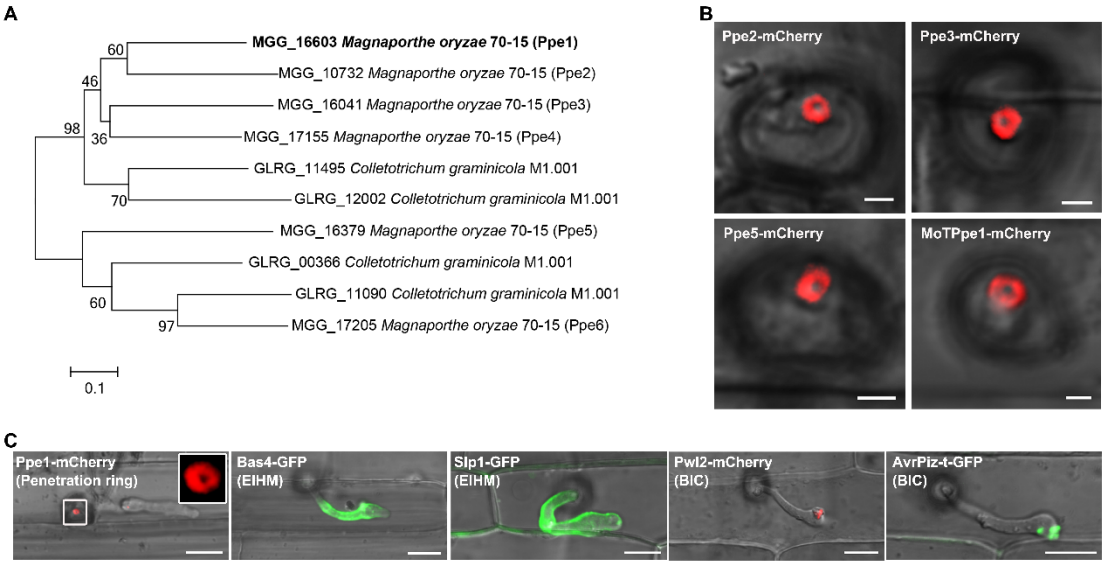

Fig. 6 Other secreted Ppe proteins also localize to the penetration ring. (A) Phylogenetic tree of Ppe1 constructed using neighbor-joining method. (B) Paralogs of Ppe1 in *M. oryzae* localize to the penetration ring. Ppe2-mCherry, Ppe3-mCherry and Ppe5-mCherry were driven by their respective native promoters. MoTPpe1-mCherry from *Magnaporthe oryzae Triticum* was expressed in *M. oryzae* (70-15), driven by its native promoter. Scale bars = 2 μm. (C) Comparison of the localization of penetration ring with those of some previously reported fungal effectors. Bas4-GFP and Slp1-GFP uniformly outlined the extra-invasive hyphal membrane (EIHM), while Pwl2-mCherry and AvrPiz-t-GFP accumulated in the biotrophic interfacial complex (BIC). Scale bars = 10 μm.

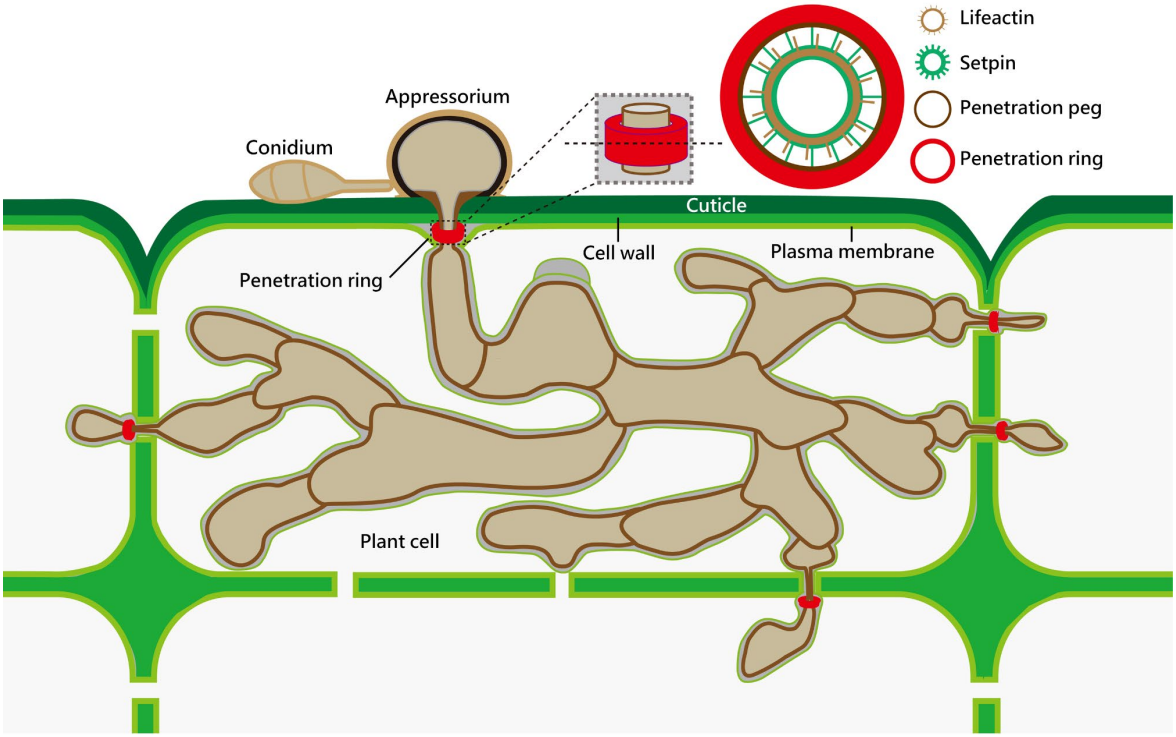

Fig. 7 A proposed working model for the discovery of penetration ring in *M. oryzae.* Penetration ring forms at the periphery of peg and accumulates fungal secreted protein such as Ppe1 to promote *M. oryzae* invasion.

730 **Supplementary figures**

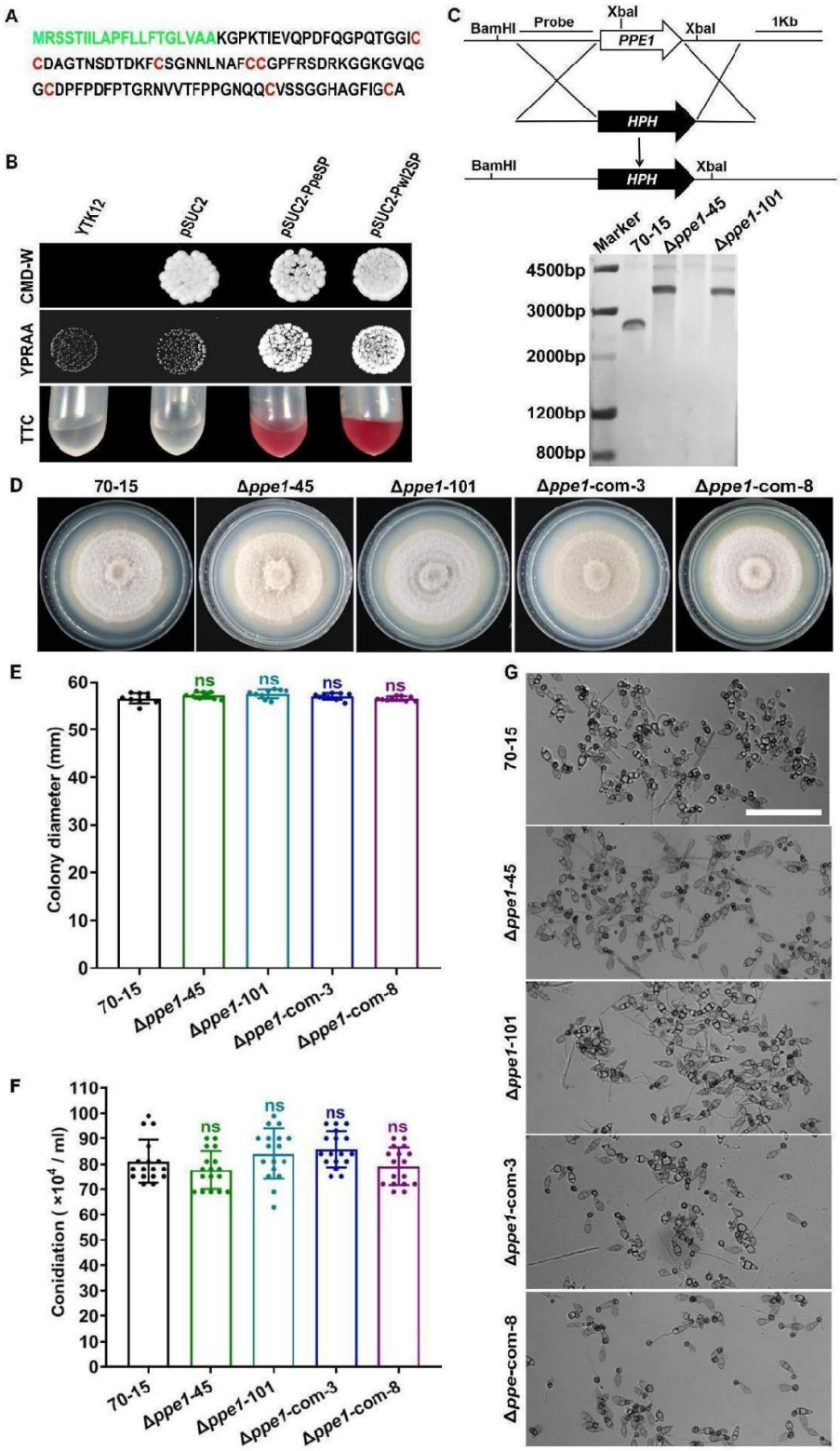

731

732 Fig. S1 Ppe1 is dispensable for mycelial growth, conidiation and appressorium formation in *M.*
733 *oryzae.* (A) Amino acid sequence of *M. oryzae* Ppe1. Signal peptides (green) were predicted by
734 Signal-5. Cysteine residues are shown in red. (B) Detection of Ppe1 signal peptide secretion by
735 yeast signal trap assay. The recombinant pSUC2-Ppe1SP and pSUC2-Pwl2SP constructs were
736 transformed into the yeast strain YTK12 respectively. The pSUC2-Pwl2SP-expressing strain
737 served as a positive control while pSUC2 empty vector was used as a negative control. (C)
738 Targeted gene deletion strategy for *PPE1* in *M. oryzae* 70-15. Schematic map showing targeted
739 disruption of *PPE1* gene via Agrobacterium tumefaciens-mediated transformation. The Southern
740 blot result shows a successful replacement of *PPE1* by single insertion of hygromycin
741 phosphotransferase (*HPH*) resistance cassette at *PPE1* ORF locus. (D) Colonies of the wild type
742 (70-15), two independent *Δppe1* transformants, and complemented strains. (E) Statistical analyses
743 of the colony diameters of each strain after being cultured on complete medium (CM) at 25 °C for
744 10 days. n = 9. (F) Statistical analyses of the number of conidia produced by each strain after being
745 cultured on CM at 25 °C for 10 days. n = 17. (G) Appressorium formation by the indicated strain
746 observed at 24 hours on artificial hydrophobic surfaces. Scale bar = 50 μm. Significant differences
747 were determined by one-way ANOVA. ns stands for no significant difference (p>0.05).

748

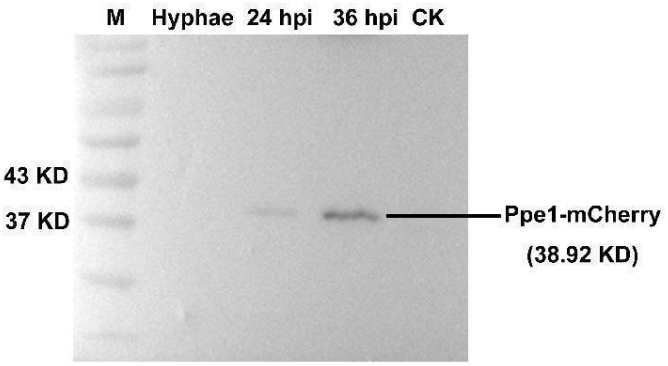

749

750 Fig. S2 Detection of Ppe1-mCherry fusion protein by western blot. M, protein marker. CK, rice
751 leaf sheaths injected with sterile double distilled water.

752

753

754

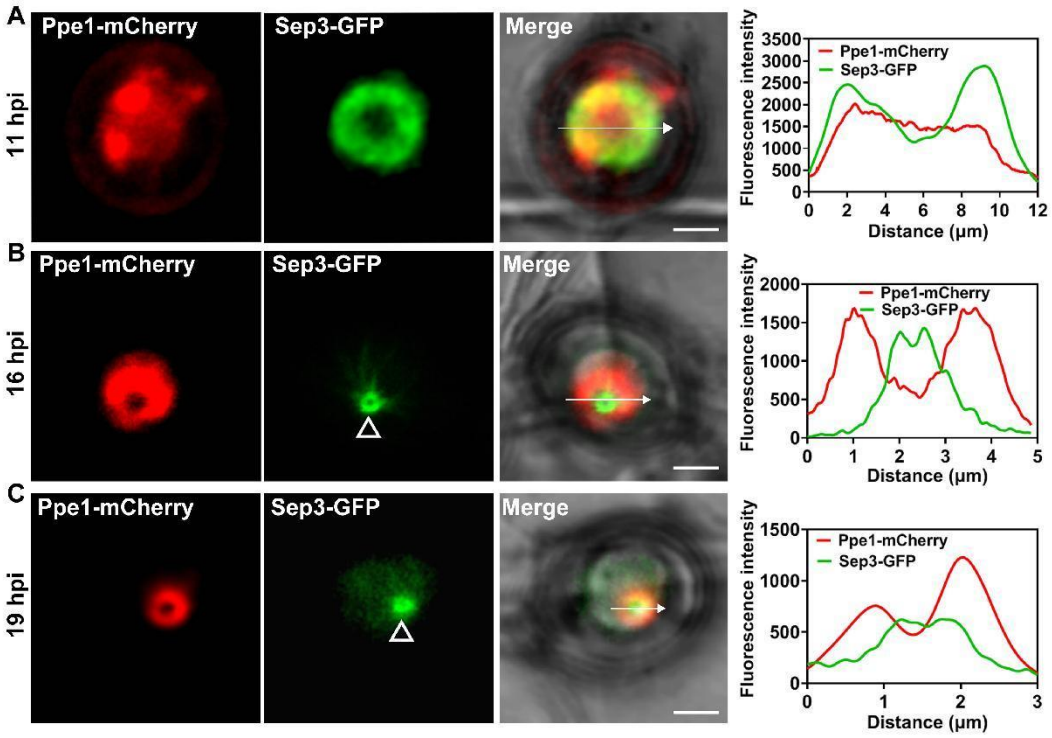

755

756 Fig. S3 Ppe1 ring is formed simultaneously with peg penetration. (A-C) Spatiotemporal dynamics
757 of Ppe1 ring and Sep3 ring during appressorium-mediated peg penetration into rice leaf sheaths.
758 Scale bars = 2 μm. Hollow triangles show the sites of penetration peg. Line graphs were generated
759 at the directions pointed by the white arrows.

760

761

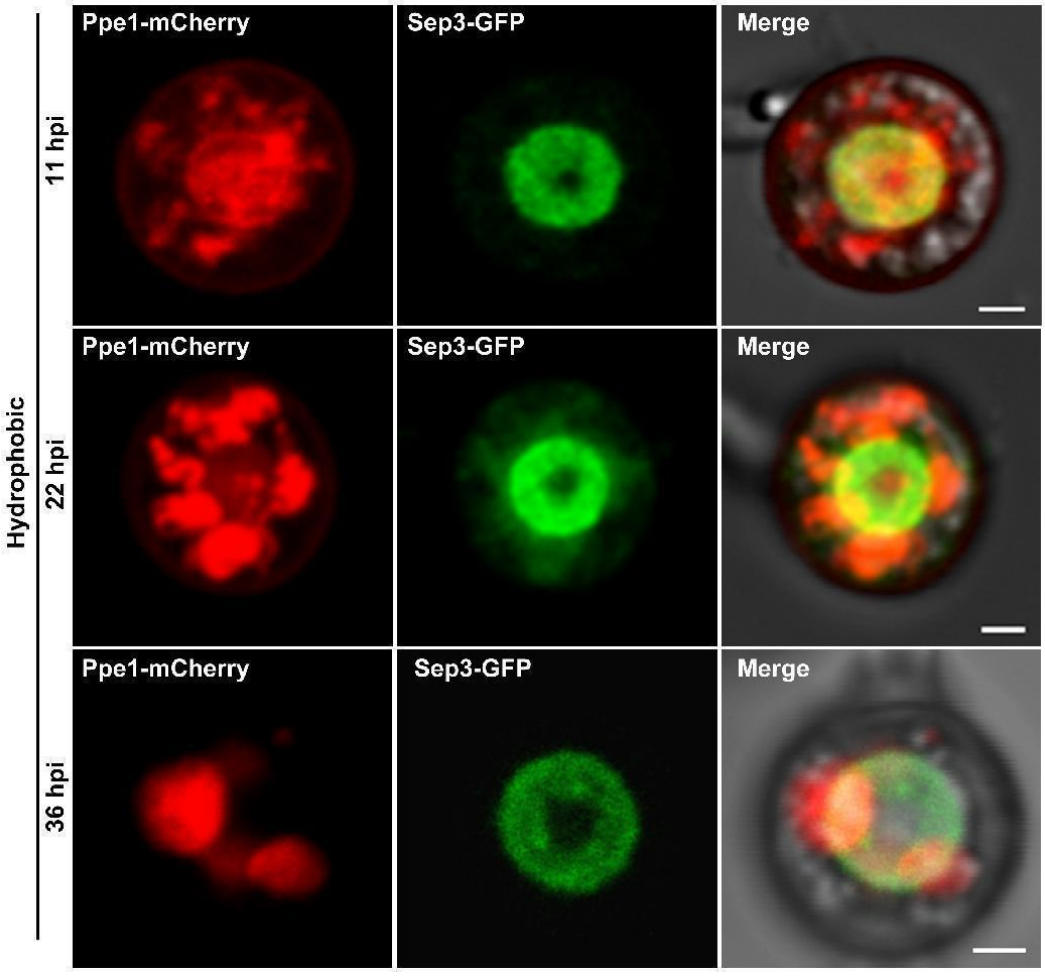

Fig. S4 Spatiotemporal dynamics of Ppe1-mCherry and Sep3-GFP on hydrophobic coverslips. Conidia were harvested from a strain co-expressing Ppe1-mCherry and Sep3-GFP and inoculated on hydrophobic coverslips and observed at each time point. Scale bars = 1 μm.

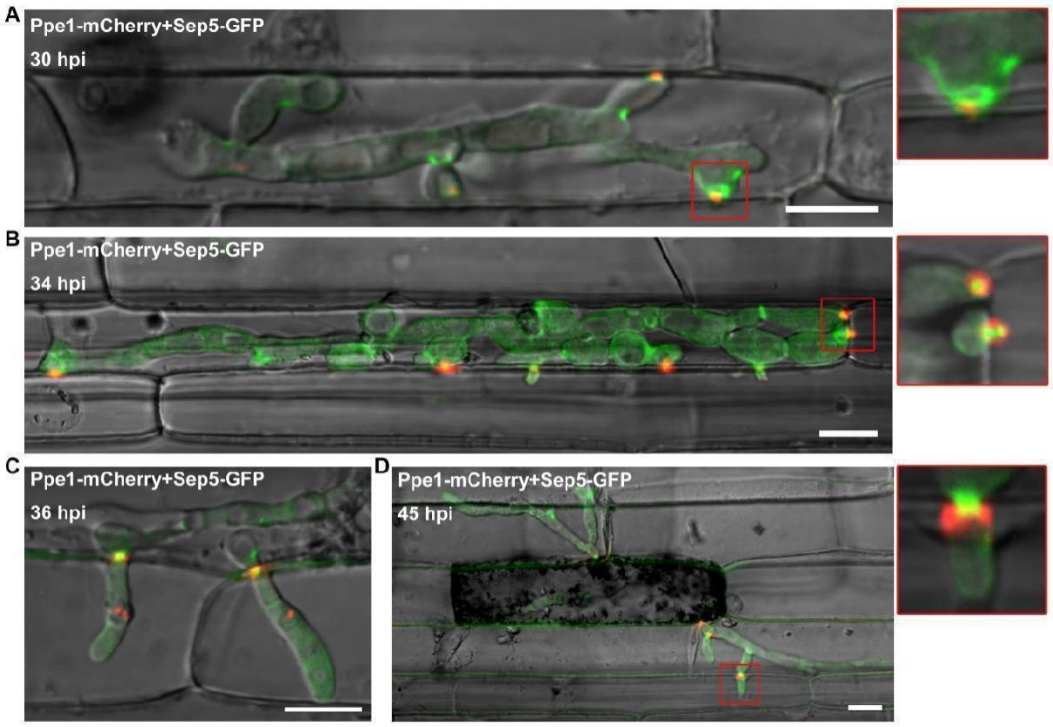

Fig. S5 Ppe1 ring was also observed during transpressorium-mediated peg penetration. (A-D) The spatiotemporal dynamics of Ppe1-mCherry and Sep5-GFP during transpressorium-mediated cell-to-cell penetration. Red squares indicate the zoomed regions, respectively. Scale bars = 10 μm.

Supplementary Videos

Video S1. 3D visualization of Ppe1-mCherry ring formation at 22 hpi.

Video S2. 3D visualization of Ppe1-mCherry and Sep3-GFP localizations at 11 hpi.

Video S3. 3D visualization of Ppe1-mCherry ring surrounding the Sep3-GFP small ring at 19 hpi.

Video S4. 3D visualization of Ppe1-mCherry ring surrounding the penetration peg at 22 hpi.

Video S5. 3D visualization of Ppe1-mCherry ring and papilla callose ring at the penetration site at 22 hpi.

781

782 **Supplementary Table S1. Fungal strains used in this study**

Strain	Description	Reference
70-15	Wild-type strain	(40)
mCherry$_{PPE1\ promoter}$	pKNT-mCherry$_{PPE1\ promoter}$ transformant of 70-15	this study
Ppe1-mCherry	pKNT-MoPpe1-mCherry and pCB1532 co-transformant of 70-15	this study
Ppe1-GFP	pKNT-MoPpe1-GFP and pCB1532 co-transformant of 70-15	this study
Ppe1-mCherry $_{situ\ insertion}$	ATMT1-Ppe1-mCherry $_{situ\ insertion}$ transformant of 70-15	this study
Sep3-GFP	Sep3-GFP transformant of Guy11	Provided by Prof. Guo Min
Sep5-GFP	Sep3-GFP transformant of Guy11	Provided by Prof. Guo Min
Ppe1-mCherry + Sep3-GFP	pKNT-Ppe1-mCherry transformant of Sep3-GFP strain	this study
Ppe1-mCherry + Sep5-GFP	pKNT-Ppe1-mCherry transformant of Sep5-GFP strain	this study
Ppe1-mCherry + Lifeact-GFP	pXY198-Lifeact-GFP transformant of Ppe1-mCherry strain	this study
Ppe1-mCherry + GFP	pKNT-RP27-GFP transformant of Ppe1-mCherry strain	this study
Δ*ppe1-45/101*	*PPE1* deletion mutant of 70-15	this study
Δ*ppe1*-com-3/8	pKNT-Ppe1-mCherry transformant of Δ*ppe1-45* mutant	this study
Δ*mst12*	*MST12* deletion mutant of Guy11	(26)
Δ*nox1*	*NOX1* deletion mutant of Ppe1-mCherry strain	this study
Δ*nox*2	*NOX2* deletion mutant of Ppe1-mCherry strain	this study
Ppe2-mCherry	pKNT-MGG_10732-mCherry transformant of 70-15	this study
Ppe3-mCherry	pKNT-MGG_16041-mCherry transformant of 70-15	this study
Ppe5-mCherry	pKNT-MGG_16379-mCherry transformant of 70-15	this study
MoTPpe1-mCherry	pKNT-MoTPpe1-mCherry transformant of 70-15	this study

PBV591	pBV591(Co-expression of Pwl2-mCherry and Bas4-GFP) transformant of 70-15	(16)
Slp1-GFP	pKNT-Slp1-mCherry transformant of 70-15	this study
AvrPiz-t-GFP	pKNT-AvrPiz-t-GFP transformant of 70-15	this study

783
784 **References**
785

786 Dean, R. A., Talbot, N. J., Ebbole, D. J., Farman, M. L., Mitchell, T. K., Orbach, M. J., Thon, M., Kulkarni,
787 R., Xu, J. R., Pan, H., Read, N. D., Lee, Y. H., Carbone, I., Brown, D., Oh, Y. Y., Donofrio, N., Jeong, J. S.,
788 Soanes, D. M., Djonovic, S., Kolomiets, E., Rehmeyer, C., Li, W., Harding, M., Kim, S., Lebrun, M. H.,
789 Bohnert, H., Coughlan, S., Butler, J., Calvo, S., Ma, L. J., Nicol, R., Purcell, S., Nusbaum, C., Galagan, J. E.,
790 & Birren, B. W., 2005, Nature 434, 980.

791 Khang, C. H., Berruyer, R., Giraldo, M. C., Kankanala, P., Park, S. Y., Czymmek, K., Kang, S., & Valent, B.,
792 2010, The Plant cell 22, 1388.

793 Park, G., Xue, C., Zheng, L., Lam, S., & Xu, J. R., 2002, Molecular plant-microbe interactions : MPMI 15,
794 183.

795

796 **Supplementary Table S2 List of Primers used in this study**
797

Primer Name	Primer Sequence (5'→3')
Construction of pSUC2 plasmid for confirming the secretory function of signal peptide (SP)	
pSUC2-Ppe1SP-F	TTTTAATTAAGAATTCATGCGTTCATCTACGATTATTCTG
pSUC2-Ppe1SP-R	CTATAGGGAGAACCTCGAGGGCGGCAACCAGGCCAGTG
pSUC2-Pwl2SP-F	TTTTAATTAAGAATTCATGAAATGCAACAACATCATCCTC
pSUC2-Pwl2SP-R	CTATAGGGAGAACCTCGAGGGCGGTTACAGTGGTCG
pSUC2-yF	ACAGATGTCGTTGTTCCAGA
Construction of plasmid for studying subcellular localization	
pKNT-Ppe1-promoter-F	AGGGAACAAAAGCTGGGTACCTCTTTCTCCCAGTCTCATC
pKNT-Ppe1-promoter-R	GCCCTTGCTCACCATAAGCTTGTTGACGCCAGGTCGTGAGA
pKNT-Ppe1-R	GCCCTTGCTCACCATAAGCTTTGCACATCCAATAAATCCAGCATGC
ATMT-mCherry$_{situ\ insertion}$-AF	GAATTCGAGCTCGGTACCGGCAACGACGACAAGAA

ATMT-mCherry$_{situ\ instertion}$-AR	GTCGACTCTAGAGGATCCATTGCACATCCAATAAATCCAGC
mCherry$_{situ\ instertion}$-F	ATGGTGAGCAAGGGCGAGGAG
mCherry$_{situ\ instertion}$-R	TTGACCTCCACTAGCTCCAGCCAAGCCCTACTTGTACAGCTCGTCCATGCC
HYG/F	GGCTTGGCTGGAGCTAGTGGAGGTCAA
HYG/R	AACCCGCGGTCGGCATCTACTCTATTC
ATMT-mCherry$_{situ\ instertion}$-BF	GAATAGAGTAGATGCCGACCGCGGGTTGTTGAGCGGAATTGCCTGTTAT
ATMT-mCherry$_{situ\ instertion}$-BR	GTCGACTCTAGAGGATCCTTCGCTTGTTGTTCTTCG
pKNT-AvrPiz-t-M-F	AGGGAACAAAAGCTGGGTACCCCAACGTAGAGCGTATGCTGT
pKNT-AvrPiz-t-M-R	GCCCTTGCTCACCATAAGCTTTTGGCGCTGAGCCTGAG
pCB1532-Slp1-G-F	ACTATAGGGCGAATTGGGTACCATTGAACAGTGCGATGCC
pCB1532-Slp1-G-R	CGCCCTTGCTCACCATAAGCTTGTTCTTGCAGATGGGGATG
GFP-sR	AGTTCACCTTGATGCCGTTC
mCherry-sR	TGGTCTTCTTCTGCATTACGG
pKNT-MoTPpe1-M-F	AGGGAACAAAAGCTGGGTACCTCTCTCAGTCTCATTCTACAGC
pKNT-MoTPpe1-M-R	GCCCTTGCTCACCATAAGCTTTGCACATCCAATAAATCCAGC
pKNT-MGG_10732-M-F	AGGGAACAAAAGCTGGGTACCGCACGTACCTTTGGTGGTTGC
pKNT-MGG_10732-M-R	GCCCTTGCTCACCATAAGCTTAGCACATCCAACATGTCCAGG
pFGL1010M-MGG_16041-M-F	CATGATGATGCTCGAGAATTCACGCCGCTTTCTGGACTA
pFGL1010M-MGG_16041-M-R	CTCGCCCTTGCTCACGGTACCGACGCATCCAACAAACCCAGGAA
pFGL1010M-MGG_16379-M-F	CATGATGATGCTCGAGAATTCTATCGTTTCGCGGGTAGATTG
pFGL1010M-MGG_16379-M-R	CTCGCCCTTGCTCACGGTACCCTTTGCGCACCCAATGAATGC
Construction of gene deletion	
ATMT-Ppe1-AF	GAATTCGAGCTCGGTACCCCACCTTTTCGTCCTCC
ATMT-Ppe1-AR	TTGACCTCCACTAGCTCCAGCCAAGCCGTTGACGCCAGGTCGTGAG

ATMT-Ppe1-BF	GAATAGAGTAGATGCCGACCGCGGGTTAGCGGAATTGCCTGTTA
ATMT-Ppe1-BR	GTCGACTCTAGAGGATCCACTGCCGACCGTGACTA
Ppe1-OF	ATGCGTTCATCTACGATTATTCTG
Ppe1-OR	TGCACATCCAATAAATCCAG
Ppe1-UA	CATCATCGCCGTCCTCT
HYG/F	GGCTTGGCTGGAGCTAGTGGAGGTCAA
HY/R	GTATTGACCGATTCCTTGCGGTCCGAA
YG/F	GATGTAGGAGGGCGTGGATATGTCCT
HYG/R	AACCCGCGGTCGGCATCTACTCTATTC
H853	GACAGACGTCGCGGTGAGTT
Nox1-AF	CACCAGATGCAGTAGTCAATT
Nox1-AR	TTGACCTCCACTAGCTCCAGCCAAGCCGTTCGTTAAAGAGCGTATGTC
Nox1-BF	GAATAGAGTAGATGCCGACCGCGGGTTGCCGAAATCTATTACGACG
Nox1-BR	CCTGAATACTTCCAAGACACC
Nox1-OF	TCACCACCTGTTTATCCCG
Nox1-OR	GACACCAATACCAGTTCCAAT
Nox1-UA	CAGAGCCACGATGCGAAAA
Nox2-AF	CGATTGTGCCTGGATGA
Nox2-AR	TTGACCTCCACTAGCTCCAGCCAAGCCGTTGCTTGGTCGGTTGTC
Nox2-BF	GAATAGAGTAGATGCCGACCGCGGGTTGAAGCAAGCCTGGCAATA
Nox2-BR	CAAAAGCCTGTTTACGAGAT
Nox2-OF	AAGATGGACGCCGCTAA
Nox2-OR	AAACGATGAAGAAGTGGTGA
Nox2-UA	ACCTCCTTGACTCTTCCACC
qRT-PCR analysis	
Ppe1-qF	TTTGCTGCGACGCTGGTA
Ppe1-qR	GGAAAATCTGGGAATGGGT
Tublin-qF	TGACAACGAGGCTCTGTACG
Tublin-qR	CCATGAAGAAGTGCAGACGA